ACTA IMEKO
ISSN: 2221-870X
*June 2025, Volume 14, Number 2, 1 - **13***

Assessing the effectiveness of sharpness metrics to determine the presence of contamination on thermographic cameras in harsh environments

Vittoria Medici[1], Milena Martarelli[1], Giuseppe Pandarese[1], Nicola Paone[1]

[1] *Department of Industrial Engineering and Mathematical Science, Università Politecnica delle Marche, Ancona, Italy*

ABSTRACT
This article assesses the effectiveness of sharpness metrics for monitoring the cleanliness of in-line thermographic systems and enabling self-diagnosis, in order to prevent degradation of metrologic performance and increase of measurement uncertainty. When optical measurement systems are installed in harsh industrial environments, external contaminants may compromise their operation conditions. Dust settling on the lens or protective window deteriorates the signal quality, reducing the sharpness of thermal images and making it challenging to extract object features accurately. This study investigates whether monitoring image sharpness can serve as an indicator of contamination presence. Contamination was simulated in controlled laboratory experiments by incrementally adding 0.4 g of dust mixture to the lens of a thermal camera observing high-temperature steel objects. Among the metrics evaluated, Histogram Entropy and the Brenner gradient showed monotonic trends and high sensitivity to small amounts of contamination, with slopes greater than 0.25. The uncertainty of these metrics is less than 0.3. The combined metric, derived through multiple linear regression, improved accuracy, with an R^2 of 0.96, up from 0.93 for Histogram Entropy and 0.95 for Brenner. Validated with real industrial data, the combined metric proved effective for real-time inline contamination diagnostics in manufacturing environments.

Section: RESEARCH PAPER

Keywords: Harsh environment; image quality assessment; infrared thermography; self-diagnosis; sharpness metric

Citation: V. Medici, M. Martarelli, G. Pandarese, N. Paone, Assessing the effectiveness of sharpness metrics to determine the presence of contamination on thermographic cameras in harsh environments, Acta IMEKO, vol. 14 (2025) no. 2, pp. 1-13. DOI: 10.21014/actaimeko.v14i2.1944

Section Editor: Antonino Quattrocchi, University of Messina, Italy

Received October 11, 2024; **In final form** November 27, 2024; **Published** June 2025

Copyright: This is an open-access article distributed under the terms of the Creative Commons Attribution 3.0 License, which permits unrestricted use, distribution, and reproduction in any medium, provided the original author and source are credited.

Funding: This work was partially supported by the OPENZDM project. This is a project from the European Union's Horizon Europe research and innovation program under Grant Agreement No. 101058673 in the call HORIZON-CL4-2021-TWIN-TRANSITION-01.

Corresponding author: Vittoria Medici, e-mail: v.medici@pm.univpm.it

1. INTRODUCTION

The issue of external contaminants affecting optical systems is particularly prevalent in harsh industrial environments or outdoor applications, where lenses are exposed to many environmental factors. Dirt on the lens is an annoyance to computer vision, and it should therefore be detected and, if possible, removed from the camera or artificially corrected on the images. Existing research has explored various techniques to address this issue across different applications, especially where image sharpness is crucial. For instance, Narasimhan and Nayar [1] developed a contrast restoration method for degraded images, demonstrating that contamination can be inferred by observing reductions in contrast and clarity. Gu et al. [2] and Zhou and Lin [3] expanded on this by examining the impact of dirt and sensor dust on image artifacts, focusing on digital image processing techniques to remove or correct these obstructions.

For instance, in the automotive sector, where visibility is paramount for safe driving, research has introduced self-detection mechanisms to identify optical contamination as a key feature for sustaining performance in foggy or particle-laden environments. Wang et al. [4] developed YOLOv5-Fog, an advanced visual detection algorithm tailored to foggy driving scenes, demonstrating how optical contamination can be managed through robust machine learning models. Advances in machine vision continue to refine such detection capabilities; Shirmohammadi and Ferrero [5] highlight the role of cameras as instruments capable of evaluating measurement reliability in real-time, bridging imaging technologies with robust data analysis. Studies like those by Tadjine et al. [6] have examined

self-diagnostic methods for vehicle cameras, focusing on algorithms that monitor image quality to notify maintenance systems of any deviation from normal operating conditions. Zhang [7] further developed autonomous systems for identifying and mitigating contaminant effects on lenses or sensors in automotive applications, a vital component for maintaining optimal performance and enhancing overall driving safety and reliability.

Infrared imaging systems are widespread in industrial settings, where they provide images used to measure temperature and/or emissivity distributions, as well as geometry, position, and motion of hot objects, with the scope of controlling process performance and/or product quality. A dirty lens on a thermographic camera installed within a production line can significantly impact the quality of the infrared image. The quality of the images generated is extremely important to obtain product information you can trust to perform quality control. In a thermal camera, dust, dirt, or moisture on the lens surface obstructs, absorbs and distorts the infrared radiation emitted by objects in the camera's field of view. This obstruction not only hampers the camera's ability to accurately capture thermal signatures but also attenuates intensity and reduces the clarity and sharpness of thermal images compromising the success of image processing. Overall, this results in degrading the quality of the measurement, both in terms of intensity and in terms of spatial distribution, in practice biasing and distorting the acquired data. Regular maintenance and cleaning of thermal camera lenses are imperative to ensure optimal imaging quality and reliable performance in various applications, including security surveillance and industrial monitoring. Therefore, detecting contamination promptly is vital to prevent compromised data integrity and ensure meaningful analysis. It could be beneficial to have metrics calculated in situ on the acquired images to determine when the system becomes contaminated, potentially compromising the integrity of the data and rendering it meaningless or soon-to-be meaningless. The goal of the analyses is a self-diagnosing machine vision system that autonomously can detect changes in its conditions [8], and can warn of the degradation of its operating condition, requiring maintenance. To achieve this goal, the authors focused on analysing the blur of acquired thermal images and then assessing the potential of sharpness metrics.

In the realm of image analysis, the assessment of image sharpness holds significant importance for researchers and practitioners alike [9]. According to [10], blur is one of the key factors that lead to quality degradation [11]. Blurring of images refers to the loss of clarity in the textures of part of the image, altering the perception of the information it contains. Several metrics for calculating image blur or, conversely, sharpness are proposed in the literature. The authors will refer indistinctly to blur metrics or sharpness metrics since sharpness and blur are inversely proportional [12]. Various sharpness methodologies have been developed to quantify and characterize image sharpness, traditionally used to assess factors such as focus [13], definition of visual content, or camera stability during image capture. Much research is based on the search for new metrics or methodologies with special interest in the topic of autofocus [14], and there is a growing interest in exploring the potential of these metrics as effective tools for Image Quality Assessment (IQA) [15]. The quantification of image quality, in this application, is strictly related to the presence of environmental contaminants. By evaluating the correlation between sharpness metrics and the presence of contaminants on lenses or optical windows, researchers aim to develop new methods for assessing and mitigating the effects of environmental factors on optical systems.

This paper explores the effectiveness of sharpness metrics as a tool for monitoring the cleanliness of in-line thermographic systems, especially in harsh industrial environments where external contaminants can significantly degrade the quality of thermal images. The study focuses on how dust and other particulates settling on the lens or protective window of these systems can blur the images, particularly when observing objects at high temperatures. The use of sharpness metrics as a diagnostic tool for thermographic systems in high temperature industrial environments in this context represents a new and practical approach. By systematically evaluating several blur metrics, typically used for focus assessment, this study uniquely addresses the need for real-time contamination monitoring tailored to the conditions of high-temperature environments. Furthermore, by combining the two most effective metrics through multiple linear regression, an advanced diagnostic tool is introduced, validated by both controlled laboratory experiments and real industry.

Through a series of laboratory experiments, where controlled amounts of dust were incrementally added to the optical window of a thermal imaging camera, the study identifies which sharpness metrics most reliably indicate the presence of contaminants. Metrics with a monotonic trend and higher sensitivity to small amounts of dirt were prioritized. The two best algorithms were combined via multiple linear regression to obtain an additional metric with increased performance. These selected metrics were then validated using data from a real industrial scenario, confirming their effectiveness in enabling the system's self-diagnosis and maintaining image quality.

This paper is structured as follows: Section 2 introduces the materials and methods used to perform image acquisition. The image processing methodology to assess the effectiveness of blur metrics to our purpose is presented in Section 3. Section 4 presents the results of the application of the algorithms, their evaluation through sensitivity analysis and uncertainty estimation, and finally their combination to increase their performance. The best performing algorithms were applied to data acquired in a real industrial scenario, and the results are shown in Section 5. Conclusions are reported in Section 6.

2. MATERIALS AND METHODS

To evaluate the effectiveness of sharpness metrics in detecting dirt on the lens of a thermal camera, the following scenario has been simulated: high-temperature steel objects are framed by a thermal camera through an infrared-transparent protective window in a harsh industrial environment. Dust gradually accumulates on the protective window over time, causing image degradation and loss of meaning of the data. Ideally, the blur indices determined from the thermal images of various objects passing through the line should not differ over time under the same boundary conditions. Metrics should increase or decrease according to the amount of contamination. In this experimental study, by keeping all external conditions unchanged, such as ambient temperature, and humidity, only the amount of dirt deposited on the lens has varied, and the sharpness of the image has been evaluated. The data obtained on the various images for different amounts of dirt are then used to evaluate the effectiveness of the different metrics.

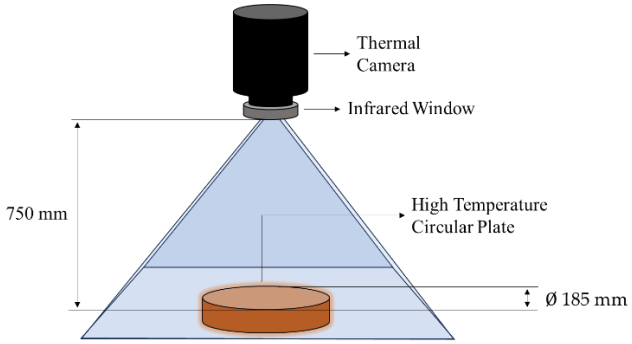

Figure 1. Scheme of the experimental setup.

2.1. Experimental setup

The thermal camera employed for the acquisition is the Testo 890, with a 640 × 480-pixel FPA micro-bolometric detector, in the spectral range of 7.5 µm to 14 µm. It can detect temperatures up to 1200 °C. The main features of the thermal camera are reported in Table 1. The infrared window, where the contaminants have been distributed, is an industrial grade of the VPFR (Viewing Pane Fixed Reinforced) Series. The optic is made of an IR transmissive polymer with a reinforcing grill made of aluminium. The thermal camera frames an area of about 490 × 370 mm².

The framed objects are a circular steel plate, which reaches a maximum temperature of 450 °C, and a squared steel plate, covered with a high emissivity black paint, which reaches a maximum temperature of 390 °C. Since many sharpness metrics rely on edge contrast, the geometry of the object's edges directly influences the metric's sensitivity and accuracy. Using both forms, the aim is to evaluate the behaviour and robustness of sharpness metrics under different geometric and thermal conditions. The circular plate provides edges in all possible directions, allowing sharpness metrics to be evaluated against a continuous edge geometry without preferred orientations. The square plate, on the other hand, introduces two primary edge directions, emphasizing directional contrasts and simulating scenarios where geometric complexity is limited to specific orientations. The square plate is a steel sheet affixed above the square plate, therefore in contrast to the circular plate, the square plate temperature is not constant but varies around the mean value: this results in a greater uncertainty of the calculated metrics. The circular plate has a diameter of 185 mm, the size of the squared plate is 200 mm. The optical window is positioned at about 750 mm from the framed plates. A schematic representation of the experimental setup is available in Figure 1. All the components are summarized in Table 1.

During data acquisition, ambient conditions recorded an approximate temperature of 23 °C and relative humidity of 40 %.

2.2. Acquisitions

The following procedure was followed for each object to acquire the images. The lens was moistened using a solution of demineralized water, and dust. Afterward, more dust was applied in a distributed manner on the lens. The dust is a mixture of black coal, iron oxides, and salts. This approach is intended to replicate the scattering behaviour of solid and fluid particles that can settle on the lens, such as dust or droplets of condensation, which is of interest due to the industrial environment considered.

A total of 11 acquisition stages were performed, beginning with the pristine condition of the lens in the initial stage, followed by ten successive stages of powder application. For each stage, 0.04 g of powder was weighed using an analytical balance with an uncertainty of ±0.005 g. The total amount of powder applied to the lens was 0.4 g, distributed evenly over the 10 application steps. The lens, with a diameter of 50 mm, has a surface area of approximately $1.96 \cdot 10^3$ mm².

At each step, the powder was distributed on the lens surface until the total amount was exhausted by the tenth stage. During each phase, after contaminants application, a sequence of 5 thermal images was systematically acquired, with a frame rate of 30 Hz.

Algorithms evaluating image sharpness were applied to these images to estimate some metrics defined in Section 3 and the uncertainty obtained (described in Section 4.2). The algorithms selected from the literature are briefly described in Section 2.3 and their expressions are available in the Appendix.

2.3. Blur metrics

This section presents the existing popular sharpness metrics which have been applied in this study. Some of them evaluate the image in the spatial domain, while others are spectral domain-based methods [16]. A more complete list of metrics to quantify the sharpness of an image can be found [17]. All these metrics implicitly consider that the presence of dirt on the lenses creates unwanted light scattering at the surface of the optics and diffraction of the wavefronts traveling the optical system, thus affecting the focusing properties and resolving power of the lens system.

The larger amount of methods in the spatial domain are based on the analysis of gradients in the image [18]. These include the Brenner function, the Tenengrad operator, and the use of the Laplacian (Variance of Laplacian or Modified Laplacian). The Brenner gradient is a fast edge detector, measuring the difference between a pixel and a neighbour that is typically two pixels away [19]. The Tenengrad operator measures the sum of the squared responses of a horizontal and a vertical Sobel mask [20]. The Laplace operator helps in detecting regions of higher contrast in the image. As an alternative to the basic version of the algorithm, it is possible to apply the Modified Laplacian or the Variance of Laplacian [16].

Table 1. List of components and specifications.

	Component	Information	Specifications
1.	Thermal camera	Testo 890 model	Image resolution: 640 × 480 pixels Spectral range: 7.5 µm to 14 µm User-defined measurement range: (0-650) °C Thermal sensitivity: < 40 mK (at 30 °C) Precision: ± 2 °C User-defined emissivity: 1.0
2.	External lens for contamination application	Viewing Pane Fixed Reinforced	Diameter: 50 cm
3.	Framed objects	Circular steel plate Squared steel plate	Diameter: 185 mm Size: 200 mm
4.	Contaminant material	Mixture of black coal, iron oxides, and salts	Total amount: 0.4 g

The image histogram, which represents how the pixel intensity values are distributed in the image, can be an indicator of sharpness. Histogram range or histogram entropy is used to quantify image blurring: sharper images contain a larger number of grey levels, and so a lower probability of occurrence of each grey level, and consequently higher entropy. Entropy is also used for machine fault diagnosis scenarios since entropy measurements are suitable for quantifying dynamic changes in the response of systems [21].

An image is sharper the more the edges of objects in the scene are evident. Therefore, other spatial methods, such as Canny and Sobel, rely on high-pass filters, commonly used in edge detection applications [22].

The main group of methods in the spectral domain is based on the Fourier transform, which converts the intensity distribution of the image into a frequency distribution function. Among them, an FFT-based method (Fast Fourier Transform) is used in this paper, which consists of calculating the energy in the high frequencies of the image summing the values of the selected frequency components. A method, proposed by [23], based on the Discrete Cosine Transform (DCT) and called DCT-QM, which stands for DCT-based Quality Degradation Metric, is also implemented. It computes the weighted average Euclidean norm in the DCT domain.

Another cluster of spectral-domain approaches is based on the statistical properties of the Discrete Wavelet Transform (DWT) coefficients. DWT decomposes the image into different scales of detail. For example, you might have one component representing finer details such as the edges of shapes, while another component might represent coarser details such as large changes in colour or brightness. Three metrics are defined in [17] based on DWT: the sum of Wavelet coefficients [24] the variance of Wavelet coefficients, and the ratio of Wavelet coefficients [25].

Many other metrics can be used to determine the sharpness of an image. For example, in this paper, the use of CPBD (Cumulative probability Blur Detection), described by [26], has been tested. CPBD is a perceptual-based objective image sharpness metric based on the cumulative probability of blur detection. It is based on the study of human perception of blur for different contrast values. It uses a probabilistic model to estimate the probability of detecting blur on each edge of the image.

Other methodologies, which have not been tested in this application, have been developed in scientific research to address the problem of evaluating image sharpness, such as the Maximum Local Variation proposed in [27], which is the maximum intensity difference between that pixel and its immediate neighbours. Other examples can be found in [16].

Each method has some advantages and disadvantages [16]. Methods in the spatial domain are the simplest and quickest to apply but are more susceptible to noise. On the other hand, methods in the frequency domain are more robust and accurate but more computationally complex and therefore less suitable for real-time applications.

In addition to these so-called traditional methods, deep learning-based approaches ([28]-[30]) have been developed with good performance, but the major disadvantage is that large amounts of data are required to increase the accuracy of the results. In this study, however, deep learning approaches have not been applied due to the limited availability of large datasets required to ensure sufficient accuracy. Instead, it was decided to rely on deterministic methods which, although less adaptive, offer a more immediate and feasible solution based on the available data.

3. IMAGE PROCESSING METHODOLOGY

To assess blur metrics efficacy, thermal images of two high-temperature objects at different amounts of contaminants on the optical window have been acquired. The objects are imaged over a cool background, to have contrasted images of the full object with its edges. 5 images for each amount of contamination have been acquired, a total of 55 images for each framed object, considering 11 stages of contamination. One sample image for each increase in the amount of dirt is shown in Figure 2 for the circular plate and in Figure 3 for the square plate.

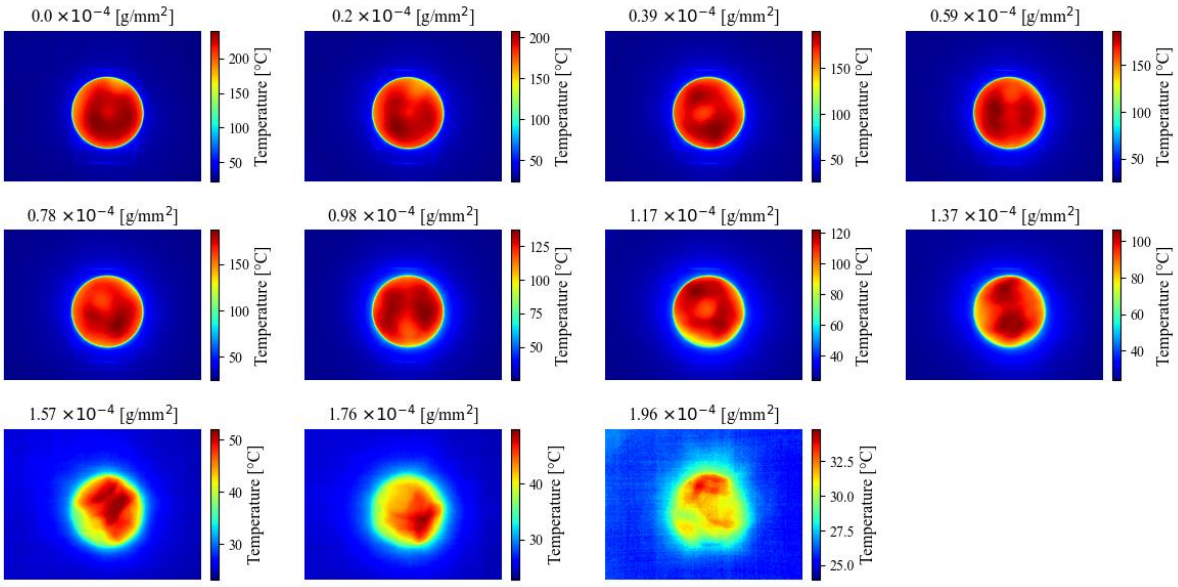

Figure 2. Thermal images of the high-temperature circular plate. Scrolling from left to right and from top to bottom, the amount of dirt on the optical window, expressed as grams per mm², increases, and the degradation of image quality is visible.

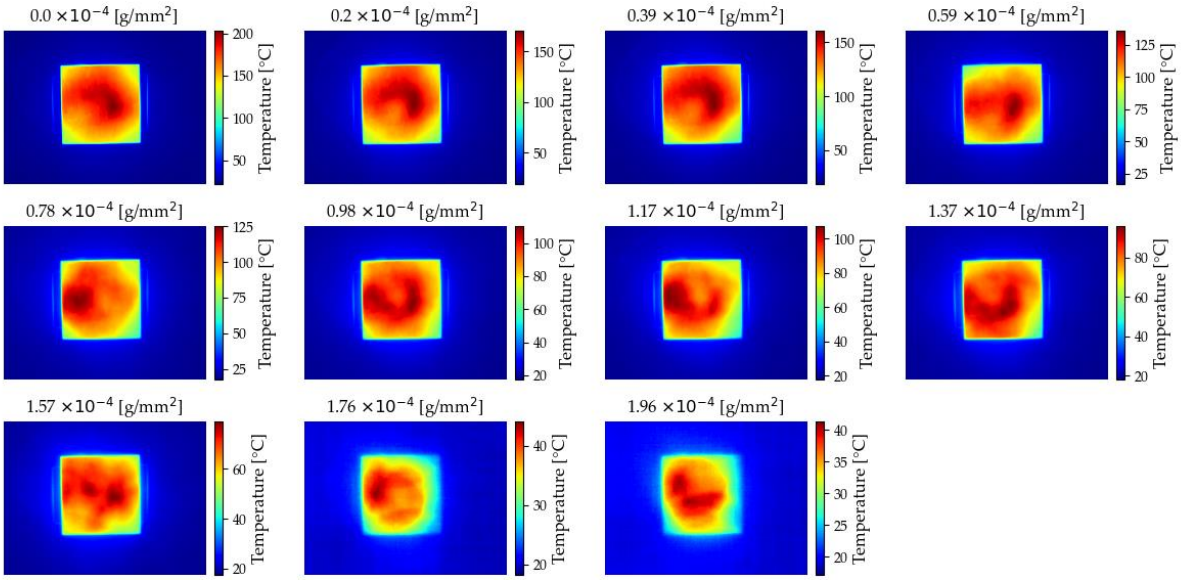

Figure 3. Thermal images of the high-temperature circular plate. Scrolling from left to right and from top to bottom, the amount of dirt on the optical window, expressed as grams per mm², increases, and the degradation of image quality is visible.

Algorithms that return a sharpness index were applied to all the images. Particularly, the following algorithms have been applied, briefly described in Section 2.3: Fast Fourier Transform, Canny, Sobel, Tenengrad, Histogram Entropy, Histogram Range, Brenner, Wavelet Sum, Wavelet Variance, Wavelet Ratio, CPBD, DCT_QM, Variance of Laplacian, Modified Laplacian. The expressions of the used metrics are available in the Appendix. Since 5 images per dirt level have been acquired, an average index value was considered in the results section, and the uncertainty is the maxima variability of values across the average value, calculated as maximum value minus minimum value.

For both objects, the change of each metric, as the amount of dirt on the lens increased, has been assessed. For each trend, monotony, and sensitivity to the presence of small amounts of dirt were evaluated. Those indices whose trends are monotonic and most sensitive were considered most fit for purpose. Processing time was used as the last metric to judge the algorithm.

Since the analysis aims to determine if these indices are suitable to determine that the camera lens is not clean, these indices must have a monotonic trend as the amount of dirt on the lens increases. Then, if the trend is monotonous, you would prefer those indices that are more sensitive to small amounts of dirt.

Thus, the derivatives of the trends of the metrics obtained were analysed first. Based on the derivatives, the monotonicity of the trends of the blur metrics can be judged. Each algorithm was then assigned a score, one for circular plate images and one for square plate images, according to the following criteria:

- Some profiles always have a negative derivative and thus are strictly monotonic. The algorithms corresponding to these profiles were assigned a score of 1.
- Other derivative profiles have small positive deviations from the y=0 axis and they are therefore considered acceptable. Algorithms corresponding to these profiles were assigned a score of 0.5.
- Some profiles have a trend far from monotonic and therefore unacceptable. These algorithms received a score of 0.

The acquisitions were made on two different objects, therefore the final score assigned to each algorithm will be given by the minimum obtained.

After defining which algorithms always have a monotonous trend, the sensitivity to small quantities of dirt has been evaluated, to understand which algorithm allows us to detect the possible presence of contaminants as promptly as possible.

To do this, the first values of the algorithms that passed the first stage of verification with a score greater than 0.5, have been interpolated with a straight line. Thus, for each algorithm, two angular coefficients were taken, one for the circular plate and one for the rectangular plate. The lower value was considered. Angular coefficients obtained for the various algorithms were compared to see which were more sensitive.

Finally, an uncertainty analysis was conducted to validate the results.

All the steps followed to identify the metrics performing the best for the dirtiness determination are summarised in the flow chart in Figure 4.

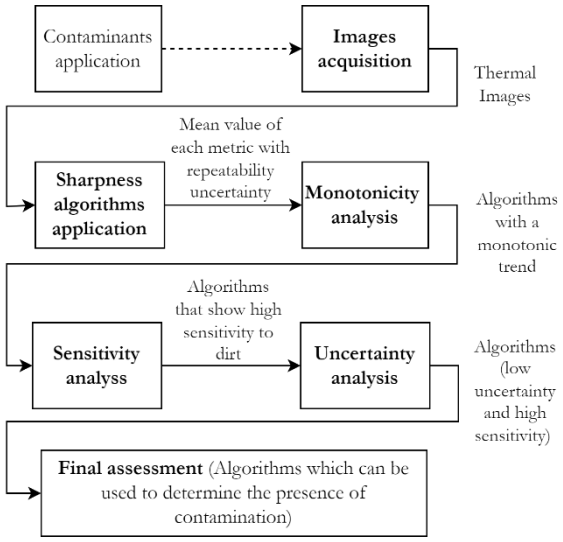

Figure 4. Flowchart of the general processing of images.

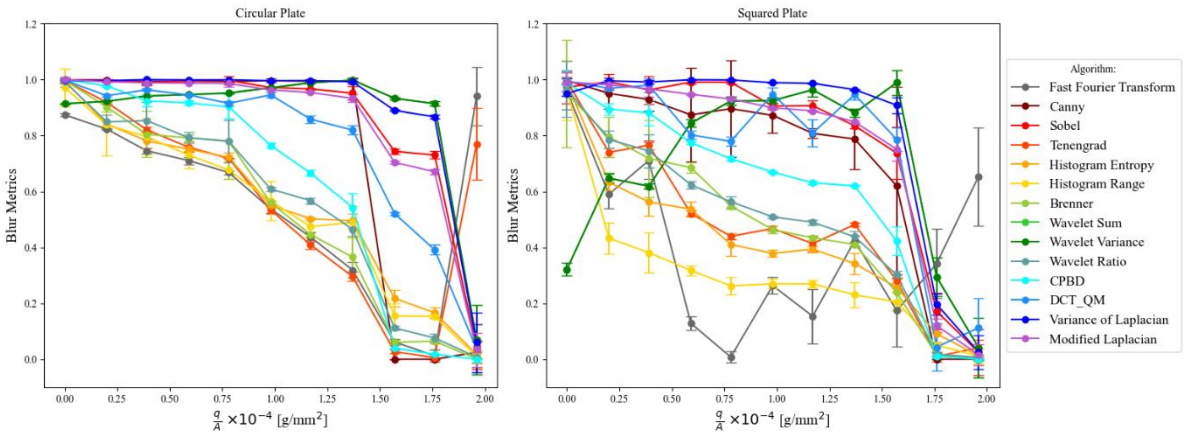

Figure 5. Blur metrics as dirtiness increases calculated on the circular plate images (left plot) and the squared plate images (right plot).

4. RESULTS

As the number of contaminants on the lens increased, various algorithms were applied to the images, and the resulting metrics can be seen in Figure 5, on the left for the circular plate, and, on the right for the square plate. The abscissa axis shows the amount of dirt in relation to the size of the lens area (g/mm^2) on which the dust has been deposited. The indices have been calculated on 5 images for each amount of contaminant. The error bar represents the uncertainty of the calculated index value for each amount of dirt, around the average value. The uncertainty is estimated as the difference between the maxima and minima values.

The sensitivity analysis is performed in Section 4.1, sing the mean value for each number of contaminants. It allows us to understand which algorithms yield an index that is particularly sensitive to the presence of dirt. Uncertainty analysis is reported in Section 4.2. Uncertainty helps to validate the efficacy of each algorithm and to understand which of the most sensitive algorithms are the most reliable and precise. In Section 4.3, the authors propose to combine two types of algorithms to improve the performance of dirtiness detection.

4.1. Sensitivity analysis

Ideally, the index values on the images should have a monotonic trend as the contaminants on the lens increase. For each set of images (circular and square plate), the monotonicity of the trends was evaluated by assigning scores to the various algorithms in accordance with what is described in the Materials and Methods section.

The assigned score can be found in Figure 6: Score 1 refers to the circular plate images and Score 2 to the squared plate. The third column of the table in the Figure 6 represents the final score, which is the minimum between the two scores.

Considering only those profiles with a monotonic trend, suitable for the proposed objective, sensitivity to small amounts of contaminant was measured. The first 6 contaminant amounts were chosen for linear regression because it is particularly important to assess the algorithm's ability to detect contaminants early, when their concentration is still low. This initial phase of contamination is crucial because the algorithm's sensitivity at this stage determines its effectiveness in identifying subtle changes. The image-related metrics for these 6 contaminant amounts were interpolated with a straight line (red bold solid lines in Figure 7), and the slope of this line represents the sensitivity of the algorithm to small amounts of contaminants.

Since the profile was obtained for two different objects, the line considered is the one with a smaller slope. The angular coefficients of the obtained straight lines are presented in Figure 8.

From this initial sensitivity analysis, among those indices with a monotonic, or near-monotonic trend, those most sensitive to the presence of small amounts of contaminants are the Histogram Entropy and Range, or the Wavelet Ratio, the Brenner filter, or the CPBD algorithm. Using such algorithms,

Algorithm	Score 1	Score 2	Final Score
Fast Fourier Transform	0	0	0
Canny	0.5	0.5	0.5
Sobel	0.5	0.5	0.5
Tenengrad	0	0	0
Histogram Entropy	1	0.5	0.5
Histogram Range	0.5	0.5	0.5
Brenner	0.5	1	0.5
Wavelet Sum	0	0	0
Wavelet Variance	0	0	0
Wavelet Ratio	0.5	1	0.5
CPBD	1	1	1
DCT_QM	0.5	0	0
Variance of Laplacian	0.5	0.5	0.5
Modified Laplacian	1	1	1

Good: Monotonous function
Good: Small deviations granted
Not good

Figure 6. Scores assigned to the metrics. Score 1 and Score 2 refer respectively to the circular and the squared plates. Scores were assigned based on the monotonicity of the function: 1 to strictly monotone functions, 0.5 functions not strictly monotone but with a few small fluctuations, 0 functions with major deviations. The Final Score considers the minimum between the two scores.

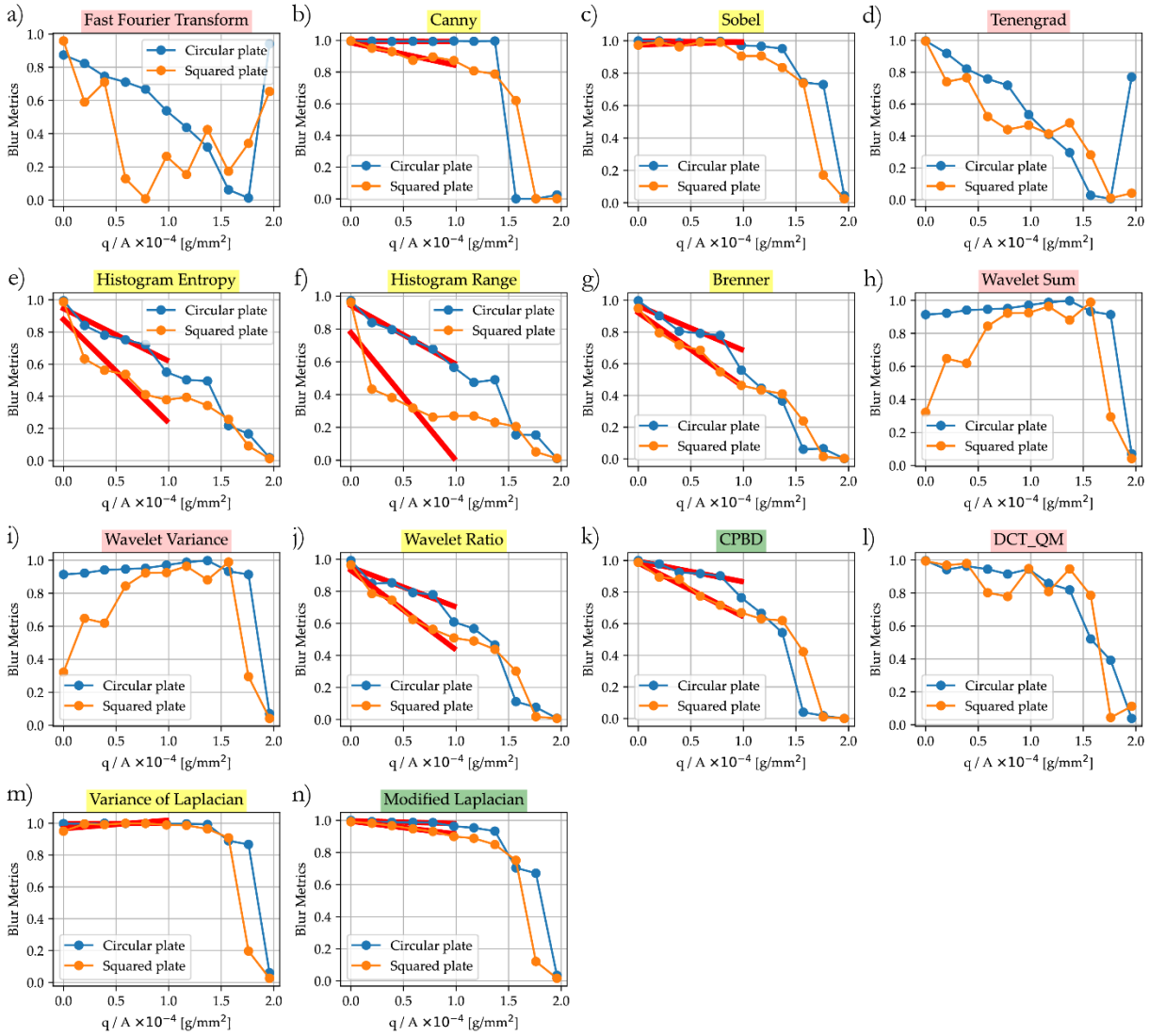

Figure 7. Sensitivity analysis. The slope of the first portion of those plots with a Final Score of at least 0.5, is analysed and represented by the fitted red lines. The abscissa axis shows the amount of dirt in relation to the size of the lens area on which the dust has been deposited. R^2 are listed here, for each image first the one for the circular plate then the one for the square plate: b) 0.61, 0.68, c) 0.67, 0.63, e) 0.70, 0.67, f) 0.77, 0.60, g) 0.69, 0.77, j) 0.66, 0.77, k) 0.74, 0.78, m) 0.65, 0.67, n) 0.68, 0.80.

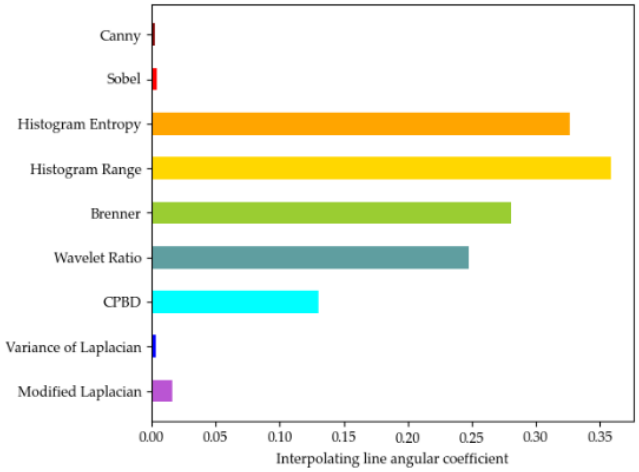

Figure 8. Angular coefficient of the fitted line for each algorithm plot. Larger values indicate larger slopes, thus larger sensitivity of the algorithm to the presence of small number of contaminants on the lens.

occlusions would be perceived to be more pronounced even for small amounts of dirt.

4.2. Uncertainty analysis

For each amount of contaminant analysed, for each object, 5 images have been acquired and on each of these the various sharpness indices have been calculated. The uncertainty of these indices is then evaluated as the range of variability (error bars in Figure 5) of the values obtained for each amount of contaminant, i.e., maximum value minus minimum value. Since the estimation of a metric is an indirect, algorithm-based measurement procedure, uncertainty is assessed through the repeatability of the measurement. This analysis was performed only on those algorithms that passed the monotonic analysis, i.e. with a final score at least 0.5.

For each amount of contaminant (thus for each uncertainty value), the compatibility from the previous measurement is evaluated, i.e., the one with less amount of contaminant. The two measurements are compatible if their respective uncertainty intervals have nonzero intersections [31]. If compatible, it might

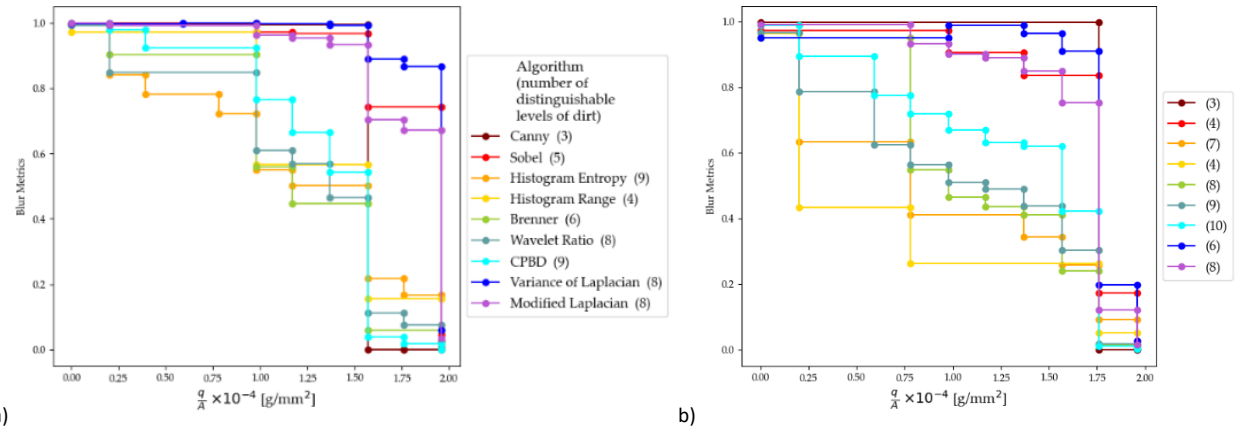

a) b)

Figure 9. Number of distinguishable levels of dirt. The trend of the various blur metrics was converted into a series of graphs indicating how many levels are distinguishable (quantified in legend) based on the compatibility of the measurements. Graph a) refers to the circular plate images. Graph b) refers to the squared plate images.

not be possible to discern the two levels of dirt; conversely, it would be possible to do so despite the uncertainty. Therefore, based on the compatibility of the measurements, the distinguishable dirt levels are defined and can be found in Figure 9. One step of the plot represents the number of mutually compatible and therefore indistinguishable levels. If, given two consecutive contamination quantity values, there are two mutually compatible measurements of the metric, then these measurements are represented by a single step. Conversely, if the successive metrics are not compatible, then they represent two discernible levels of dirt. The number of distinguishable dirt levels can be considered an indicator of the resolution of the algorithm.

Finally, the combined standard uncertainty is calculated to get a general picture of the performance of each algorithm. It has been calculated according to equation (1). The obtained combined uncertainties are shown in Figure 10.

$$u_c = \sqrt{u(q_1)^2 + \cdots + u(q_n)^2} \tag{1}$$

$u(q_i)$ is the uncertainty of the algorithm associated with the quantity of contaminant on the lens.

The results of the sensitivity analysis were put together with those of the uncertainty analysis for all the indices considered. The graph in Figure 11 shows the relationship between the sensitivity, to the presence of small amounts of contaminants on the lens, of the algorithms and the combined standard uncertainty. The green box contains those algorithms for which the sensitivity is sufficiently high, and the uncertainty is smaller.

The algorithms considered best due to greater sensitivity to small amounts of dirt and low uncertainty are Histogram Range, Histogram Entropy, Brenner, and the ratio of wavelet coefficients. Furthermore, these algorithms have a computation time for a single image of less than 5 ms, making them suitable for real-time use in high-speed manufacturing environments. Their low computational delay ensures that they can be integrated into fast-paced production lines where data acquisition rates are high, allowing for immediate feedback and decision-making.

4.3. Metrics combination for dirtiness sensitivity improvement

To achieve better performance in defining the level of dirtiness, two metrics were combined using multiple linear regression: the Histogram Entropy, which reflects the contrast and overall complexity of the image, and the Brenner gradient, which captures the sharpness and edge definition. These metrics target different aspects of image quality, ensuring a more robust assessment of dirtiness. Repeatability uncertainties in the data were taken into account during the regression process, using weights inversely proportional to the square of the uncertainty. Weighted Least Squares (WLS) methods use these weights to better fit the line or plane to the data. In practice, regression attempts to minimize the sum of the weighted errors.

The line or plane resulting from the weighted regression will be more influenced by data with low uncertainties (i.e., those that are more reliable). This helps to obtain a model that improves the estimation of contamination by considering the

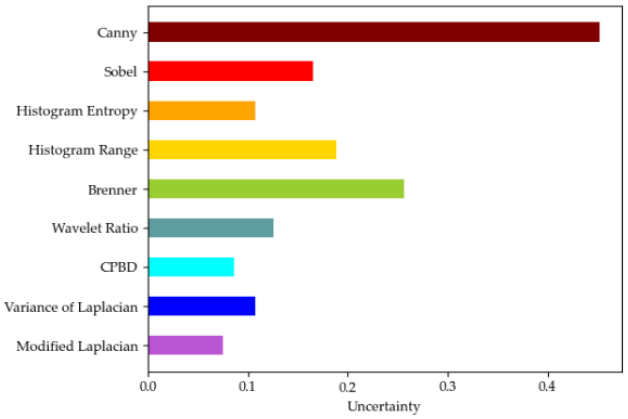

Figure 10. Combined standard uncertainty associated with each algorithm.

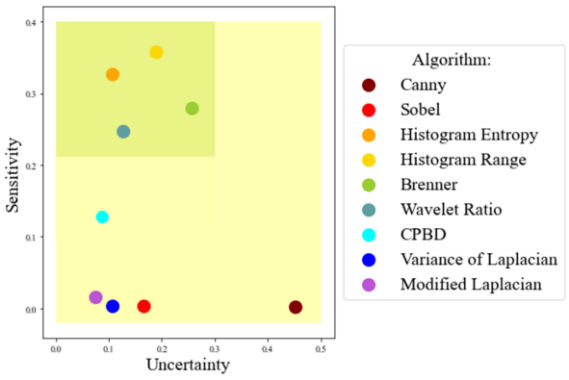

Figure 11. Sensitivity and uncertainty of those algorithms with a monotonous trend

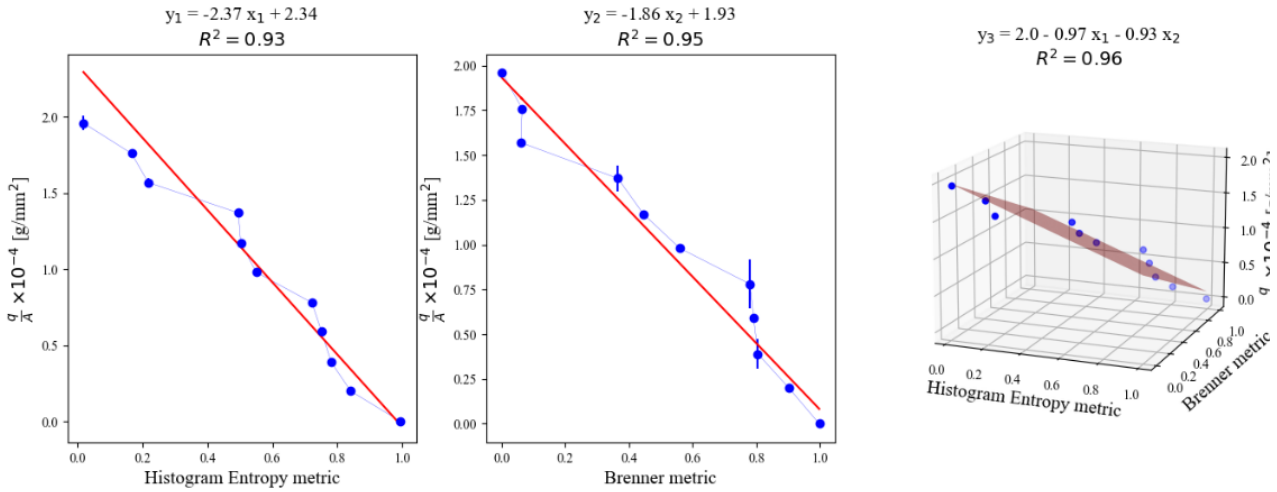

Figure 12. Correlation of dirt quantities with single metrics and combined metrics. On the left is the correlation between the Histogram Entropy metric and the amount of dirt. In the centre, the correlation between the Brenner metric with the amount of dirt. On the right, the correlation between the amount of dirt and the combination of the two metrics by multiple linear regression.

reliability of the data. This approach allowed the complementary strengths of each metric to be exploited, improving the overall predictive power. The final model demonstrated improved performance, as evidenced by a higher R-squared value, indicating a better fit to the data and more accurate estimation of the level of dirt.

The combined model used is that in equation (2).

$$y = \gamma_0 + \gamma_1 x_1 + \gamma_2 x_2 \, . \tag{2}$$

The linear regression equations used for the single metrics are available in equation (3) and (4):

$$y = \alpha_0 + \alpha_1 x_1 \tag{3}$$

$$y = \beta_0 + \beta_1 x_2 \, , \tag{4}$$

where y is the quantity of contamination to be predicted, x_i denotes the i-th independent variable, which corresponds to the value of the i-th metric used in the regression (i.e., x_1 for the Histogram Entropy and x_2 for the Brenner metric), α_0, β_0 and γ_0 are the intercepts of each respective model, representing the value of y when all other variables are set to zero. α_1, β_1 and γ_1, γ_2 are the regression coefficients associated with each independent variable. These coefficients indicate the influence of each metric on the predicted contamination level: the higher the value of a coefficient, the greater the impact of the corresponding metric on the estimation of y. The higher the i-th coefficient is, the greater the effect of the i-th dependent variable on the variable x to be predicted.

When modelling the value of a metric linearly with respect to increasing lens contamination (Figure 12), an R^2 of 0.93 (Histogram Entropy) and an R^2 0.95 (Brenner) are obtained. Combining the two metrics, via multiple linear regression, the plan obtained has an R^2 of 0.96. Thus, the performance of the maintenance system, which warns of the amount of dirt present, is improved.

To validate the adequacy of the regression model, an analysis of residuals was performed. Figure 13 shows the residuals plotted against the predicted values. The random distribution of residuals around zero indicates that the model fits the data well, with no obvious patterns or systematic errors.

5. APPLICATION TO REAL MANUFACTURING DATA

The algorithms found to be the best from the analysis were applied to real data acquired within a manufacturing plant with a harsh environment. The data are thermal images of steel bars at temperatures above 1000 °C. Data were acquired with the Optris PI 1M [32] thermal camera in the NIR (near-infrared) spectrum (0.85-1.1 μm), which is part of the Non-Destructive Inspection system (NDI) described in [33]. According to [34], the emissivity was set at 0.85, calibrated using a known black paint with high emissivity as a reference, applied to a part of the sample, which was heated to approximately 1000 °C.

The acquired data refers to three different days (not sequential) when the levels of dirt on the lens were visually inspected, as exact quantification was not feasible due to the harsh environment. At the end of the analysis, the real condition of the lens was visually verified, as shown in Figure 14, confirming the complete coverage of dust. However, data from intermediate days are not available due to production interruptions.

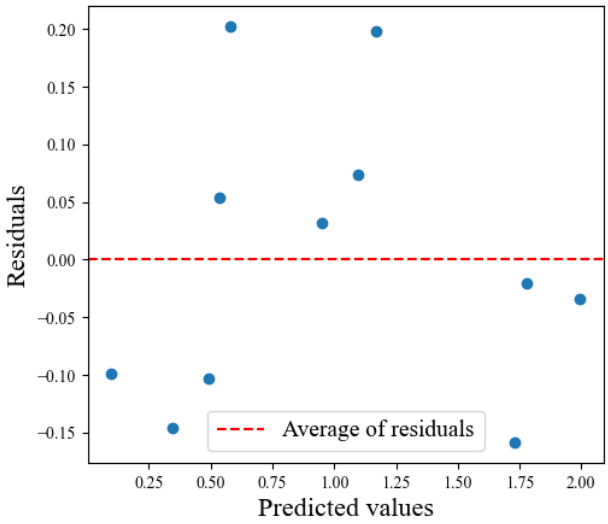

Figure 13. Residuals analysis. The residuals are obtained from the difference between the value predicted by the combined model and the actual contaminant quantity values.

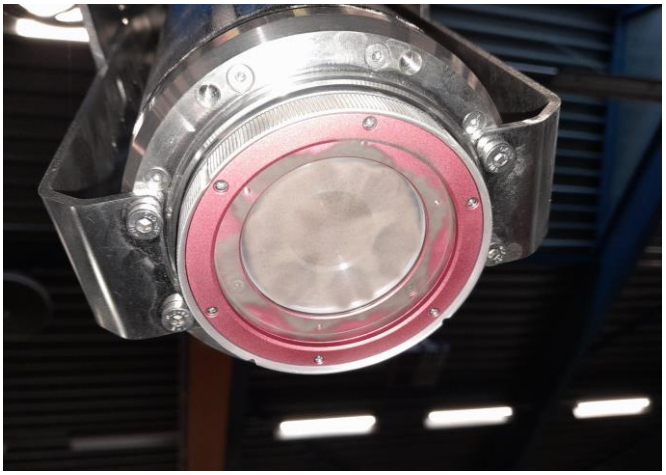

Figure 14. Visual inspection of the lens at the end of the analysis, showing complete dust coverage.

- On the first day, the indices confirm that the thermal images are perfectly sharp (Figure 15 a), as no dust was deposited on the lens of the thermal camera.
- On the second day, one week later, the indices began to decrease, corresponding to partial blurring of the thermal images caused by dirt partially occluding the lens (Figure 15 b).
- By the third day, about 10 days later, the indices reached their lowest values, indicating that dust had completely covered the lens. The resulting image was significantly blurred, as shown in the (Figure 15 c), making it challenging to extract geometric features from the object.

Histogram Entropy, and Brenner algorithms have been applied to these three sets of images. Also, the combination of these two algorithms have been applied. Resulting metrics are shown in Figure 16. The graphs show the values of these metrics for various products. The decrease in the index as the number of contaminants increases is clear, so these metrics are confirmed to be valid to assess the quality of thermal images inline.

These analyses on real-time data allowed to validate the approach under varying levels of environmental factors, such as ambient noise, temperature fluctuations, and humidity, which are common in industrial settings. By applying the sharpness metrics to data acquired under these diverse conditions, the robustness and adaptability of the algorithms have been demonstrated, confirming their effectiveness in assessing the quality of thermal images even in environments with unpredictable and challenging variables.

6. CONCLUSIONS

The performance of optical systems installed in hostile environments is likely to be compromised by the presence of external contaminants. This is particularly true for imaging systems used to take measurements in harsh environments. In the study presented in this paper, the authors set out to assess what metrics might help detect abnormal conditions in the operation of a thermographic inspection system due to the deposition of contaminants on the external optical window. The presence of dirt alters the passage of infrared radiation from framed high-temperature objects, resulting in a loss of image sharpness. By monitoring this sharpness and exploiting algorithms that are typically used to define the focus of cameras, it is possible to obtain indicators that can be used to maintain the system.

In the laboratory, the optical window of a thermal imaging camera was contaminated by adding small amounts of dust at a time. A series of images were then acquired for each amount of dirt, and different algorithms were applied to obtain sharpness indices. The trend of these metrics as the amount of dirt increased was analysed, and those metrics with a monotonic trend and more sensitive to the presence of small amounts of

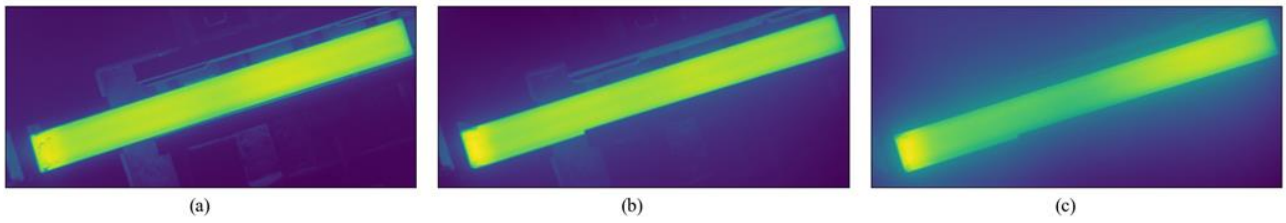

Figure 15. Example images from the 3 days of production. a) Clean lens. b) Partial occlusion of the lens by dirt. c) Dirty lens.

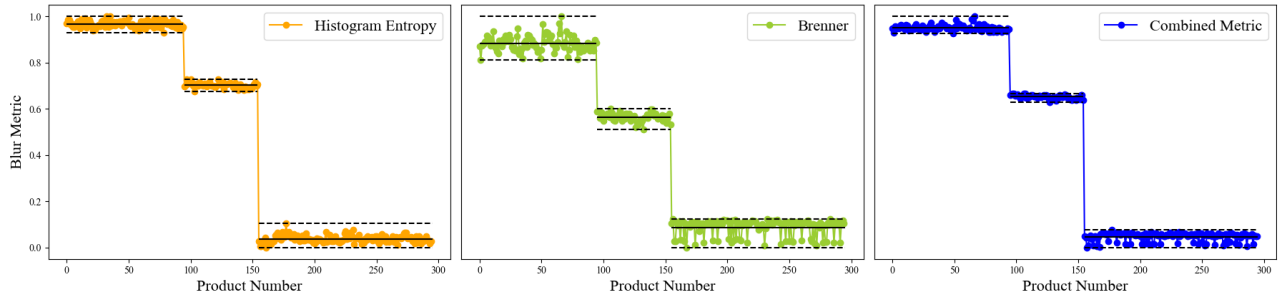

Figure 16. Blur Metrics calculated on production data. Data with product numbers 0 to 94 refer to the first data set (clean lens), 94 to 154 refer to the second data set (partially dirty lens), and 154 to 290 refer to the second data set (partially dirty lens). The black lines represent the average value of the respective soiling level and dashed, the range of variability given by maximum values and minimum values. On the left, Histogram Entropy algorithm has been applied, on the centre Brenner, and on the left the combined metric.

dirt were then conditioned better. Uncertainty analysis allowed some metrics to be further discarded.

Sensitivity and uncertainty analysis allowed to select the best algorithms from the initial list: Histogram Entropy, Range and the Brenner algorithm. Furthermore, these algorithms have been combined to improve the accuracy of the diagnostic tool. This combined metric was validated using data from a real industrial scenario, demonstrating its robustness and adaptability for real-time inline contamination diagnostics in manufacturing environments. The proposed approach confirms the potential of the selected metrics to enable effective, in-situ diagnostics, preserving the integrity of thermographic inspection systems even under harsh conditions.

ACKNOWLEDGEMENT

This work was partially supported by the OPENZDM project. This is a project from the European Union's Horizon Europe research and innovation program under Grant Agreement No. 101058673 in the call HORIZON-CL4-2021-TWIN-TRANSITION-01.

APPENDICES

Blur metrics expressions are described in this section.

FFT (Fast Fourier Transform)

Uses the Fourier transform to convert the image into the frequency domain. Sharpness is evaluated by summing the high-frequency components

$$FFT_{\text{sharpness}} = \sum_{i,j} |F(i,j)| \,,$$

where F is the Fourier transforms on the image.

Canny filter

Uses the Canny edge detection algorithm to determine sharpness based on the number of detected edges

$$Canny_{\text{sharpness}} = \sum_{i,j} Canny\ (i,j).$$

Sobel filter

Applies the Sobel filter to calculate horizontal and vertical gradients, combining the results to obtain a measure of sharpness

$$Sobel_{\text{sharpness}} = \sum_{i,j} \sqrt{(G_x(i,j))^2 + \left(G_y(i,j)\right)^2} \,,$$

where G_x and G_y and the Sobel gradients in the horizontal and vertical directions.

Tenengrad operator

Similar to the Sobel method but squares the gradient values to emphasize stronger variations

$$Tenengrad_{\text{sharpness}} = (G_x(i,j))^2 + \left(G_y(i,j)\right)^2 .$$

Histogram Entropy

Calculates the entropy of the image's histogram, measuring the amount of information or detail

$$Hist-entropy_{\text{sharpness}} = -\sum_{k} p(k)\log_2\big(p(k)\big) \,,$$

where $p(k)$ is the probability of grayscale level k.

Histogram Range

Measures the range of values in the histogram by calculating the difference between the maximum and minimum histogram values

$$Hist-range_{\text{sharpness}} = \max(hist) - \min(hist) \,.$$

Brenner

Calculates sharpness based on the difference between pixels two units apart in both horizontal and vertical directions

$$Brenner_{\text{sharpness}} = \frac{1}{M \cdot N}\sum_{i,j} \max\Big((I(i+2,j) - I(i,j))^2, \big(I(i,j+2) - I(i,j)\big)^2\Big) \,,$$

where M and N are the height and width of the image.

Wavelet Sum

Uses the wavelet transform to calculate the energy in the detail subbands

$$Wav-sum_{\text{sharpness}} = \sum_{i,j} (cH(i,j)^2 + cV(i,j)^2 + cD(i,j)^2) \,,$$

where cH, cV, and cD are the wavelet coefficients of the horizontal, vertical, and diagonal components.

Wavelet Variance

Calculates the variance of the detail subbands in the wavelet transform

$$Wav-var_{\text{sharpness}} = \text{Var}(cH) + \text{Var(cV)} + \text{Var(cD)} \,.$$

Wavelet Ratio

Calculates the ratio of the sum of the horizontal and vertical components to the diagonal component in the wavelet transform

$$Wav-ratio_{\text{sharpness}} = \frac{\sum_{\text{i,j}}|cH(i,j)| + \sum_{\text{i,j}}|cV(i,j)|}{\sum_{\text{i,j}}|cD(i,j)|} \,.$$

CPBD (Cumulative Probability of Blur Detection)

Uses the standard deviation and mean gradient to estimate the cumulative probability of blur detection

$$CPBD_{\text{sharpness}} = 1 - \left(\frac{1}{1 + \exp\left(-\left(\frac{\sigma_g}{\mu_g \sqrt{2}} - t \right) \right)} \right),$$

where σ_g is the standard deviation of the gradient, μ_g is the mean gradient, and t is the threshold. The threshold value was set to 0.75, determining how much an image must deviate from average gradients to be considered blurry.

DCT-QM (Discrete Cosine Transform Quality Metric)

Uses the discrete cosine transform to calculate sharpness as a normalized norm

$$DCT_{QM_{\text{sharpness}}} = \frac{\|DCT(I)\|}{\sqrt{N} - 1},$$

where DCT(I) is the discrete cosine transform of the image and N is the image size.

Variance of Laplacian

Calculates the variance of the image filtered with the Laplacian kernel to measure sharpness.

$$Var - Laplacian_{\text{sharpness}} = \text{Var}\big(Laplacian(I)\big).$$

Modified Laplacian

Applies a modified Laplacian filter and calculates the sum of the absolute values of the results to estimate sharpness.

$$Mod - Laplacian_{\text{sharpness}} = \frac{1}{M \cdot N} \sum_{i,j} |L_x(i,j)| + \left|L_y(i,j)\right|,$$

where L_x and L_y are the responses of the modified Laplacian filter in the horizontal and vertical directions.

REFERENCES

[1] S. G. Narasimhan, S. K. Nayar, Contrast restoration of weather degraded images, IEEE Trans. Pattern Anal. Mach. Intell., vol. 25, no. 6, June 2003, pp. 713–724.
DOI: https://doi.org/10.1109/TPAMI.2003.1201821

[2] J. Gu, R. Ramamoorthi, P. Belhumeur, S. Nayar, Removing image artifacts due to dirty camera lenses and thin occluders, ACM Trans. Graph., vol. 28, no. 5, Dec. 2009, pp. 1–10.
DOI: https://doi.org/10.1145/1618452.1618490

[3] C. Zhou, S. Lin, Removal of Image Artifacts Due to Sensor Dust, IEEE Conf. on Computer Vision and Pattern Recognition, Minneapolis, MN, USA, 17-22 Jun. 2007, pp. 1–8.
DOI: https://doi.org/10.1109/CVPR.2007.383260

[4] H. Wang, Y. Xu, Y. He, Y. Cai, L. Chen, Y. Li, M. A. Sotelo, Z. Li, YOLOv5-Fog: A Multiobjective Visual Detection Algorithm for Fog Driving Scenes Based on Improved YOLOv5, IEEE Trans. Instrum. Meas., vol. 71, 2022, pp. 1–12.
DOI: https://doi.org/10.1109/TIM.2022.3196954

[5] S. Shirmohammadi, A. Ferrero, Camera as the instrument: the rising trend of vision based measurement, IEEE Instrum. Meas. Mag., vol. 17, no. 3, Jun. 2014, pp. 41–47.
DOI: https://doi.org/10.1109/MIM.2014.6825388

[6] H. Tadjine, D. Anoushirvan, D. Eugen, K. Schulze, Optical Self Diagnostics for Camera Based Driver Assistance, Proc. of the FISITA 2012 World Automotive Congress, vol. 197, SAE-China and FISITA, Eds., in Lecture Notes in Electrical Engineering, vol. 197, Berlin, Heidelberg: Springer Berlin Heidelberg, 2013, pp. 507–518.
DOI: https://doi.org/10.1007/978-3-642-33805-2_40

[7] Y. Zhang, Self-detection of optical contamination or occlusion in vehicle vision systems, Opt. Eng., vol. 47, no. 6, Jun. 2008, p. 067006.
DOI: https://doi.org/10.1117/1.2947578

[8] J. E. Amadi-Echendu, Hengjun Zhu, Detecting changes in the condition of process instruments, IEEE Trans. Instrum. Meas., vol. 43, no. 2, Apr. 1994, pp. 355–358.
DOI: https://doi.org/10.1109/19.293447

[9] R. Ferzli, L. J. Karam, No-reference objective wavelet based noise immune image sharpness metric, IEEE Int. Conf. on Image Processing 2005, Genova, Italy, 2005, p. I–405.
DOI: https://doi.org/10.1109/ICIP.2005.1529773

[10] H. Tong, M. Li, H. Zhang, Ch. Zhang, Blur detection for digital images using wavelet transform, IEEE Int. Conf. on Multimedia and Expo (ICME) (IEEE Cat. No.04TH8763), Taipei, Taiwan, 27-30 June 2004, pp. 17–20.
DOI: https://doi.org/10.1109/ICME.2004.1394114

[11] A. Lavatelli, E. Zappa, Uncertainty in vision based modal analysis: probabilistic studies and experimental validation, Acta IMEKO, vol. 5, no. 4, Dec. 2016, p. 37-48.
DOI: https://doi.org/10.21014/acta_imeko.v5i4.426

[12] R. Ferzli, L. J. Karam, A No-Reference Objective Image Sharpness Metric Based on the Notion of Just Noticeable Blur (JNB), IEEE Trans. Image Process., vol. 18, no. 4, Apr. 2009, pp. 717–728.
DOI: https://doi.org/10.1109/TIP.2008.2011760

[13] L. Firestone, K. Cook, K. Culp, N. Talsania, K. Preston, Comparison of autofocus methods for automated microscopy, Cytometry, vol. 12, no. 3, Jan. 1991, pp. 195–206.
DOI: https://doi.org/10.1002/cyto.990120302

[14] Bin Yang, Shutao Li, Multifocus Image Fusion and Restoration With Sparse Representation, IEEE Trans. Instrum. Meas., vol. 59, no. 4, Apr. 2010, pp. 884–892.
DOI: https://doi.org/10.1109/TIM.2009.2026612

[15] D. M. Chandler, Seven Challenges in Image Quality Assessment: Past, Present, and Future Research, Int. Sch. Res. Not., vol. 2013, Feb. 2013, p. e905685.
DOI: https://doi.org/10.1155/2013/905685

[16] M. Zhu, L. Yu, Z. Wang, Z. Ke, C. Zhi, Review: A Survey on Objective Evaluation of Image Sharpness, Appl. Sci., vol. 13, no. 4, Feb. 2023, p. 2652.
DOI: https://doi.org/10.3390/app13042652

[17] S. Pertuz, D. Puig, M. A. Garcia, Analysis of focus measure operators for shape-from-focus, Pattern Recognit., vol. 46, no. 5, May 2013, pp. 1415–1432.
DOI: https://doi.org/10.1016/j.patcog.2012.11.011

[18] F. Kou, W. Chen, C. Wen, Z. Li, Gradient Domain Guided Image Filtering, IEEE Trans. Image Process., vol. 24, no. 11, Nov. 2015, pp. 4528–4539.
DOI: https://doi.org/10.1109/TIP.2015.2468183

[19] S. Yazdanfar, K. B. Kenny, K. Tasimi, A. D. Corwin, E. L. Dixon, R. J. Filkins, Simple and robust image-based autofocusing for digital microscopy, Opt. Express, vol. 16, no. 12, Jun. 2008, p. 8670.
DOI: https://doi.org/10.1364/OE.16.008670

[20] F. S. Helmli, S. Scherer, Adaptive shape from focus with an error estimation in light microscopy, in ISPA 2001. Proc. of the 2nd Int. Symp. on Image and Signal Processing and Analysis, in conjunction with 23rd Int. Conf. on Information Technology Interfaces (IEEE Cat. No.01EX480), Pula, Croatia, 19-21 June 2001, pp. 188–193.
DOI: https://doi.org/10.1109/ISPA.2001.938626

[21] Z. Huo, M. Martinez-Garcia, Y. Zhang, R. Yan, L. Shu, Entropy Measures in Machine Fault Diagnosis: Insights and Applications, IEEE Trans. Instrum. Meas., vol. 69, no. 6, Jun. 2020, pp. 2607–2620.
DOI: https://doi.org/10.1109/TIM.2020.2981220

[22] I. Bölkény, Artificial Neural Network-based detection of gas hydrate formation, Acta IMEKO, vol. 10, no. 3, Sep. 2021, p. 117-124.
DOI: https://doi.org/10.21014/acta_imeko.v10i3.1060

[23] S.-H. Bae, M. Kim, DCT-QM: A DCT-Based Quality Degradation Metric for Image Quality Optimization Problems, IEEE Trans. Image Process., vol. 25, no. 10, Oct. 2016, pp. 4916–4930.
DOI: https://doi.org/10.1109/TIP.2016.2598492

[24] Ge Yang, B. J. Nelson, Wavelet-based autofocusing and unsupervised segmentation of microscopic images, Proc. Of the 2003 IEEE/RSJ Int. Conf. on Intelligent Robots and Systems (IROS 2003) (Cat. No.03CH37453), Las Vegas, Nevada, USA, 27-31 October 2003, pp. 2143–2148.
DOI: https://doi.org/10.1109/IROS.2003.1249188

[25] H. Xie, W. Rong, L. Sun, Wavelet-Based Focus Measure and 3-D Surface Reconstruction Method for Microscopy Images, in 2006 IEEE/RSJ Int. Conf. on Intelligent Robots and Systems, Beijing, China, 9-15 October 2006, pp. 229–234.
DOI: https://doi.org/10.1109/IROS.2006.282641

[26] N. D. Narvekar, L. J. Karam, A No-Reference Image Blur Metric Based on the Cumulative Probability of Blur Detection (CPBD), IEEE Trans. Image Process., vol. 20, no. 9, Sep. 2011, pp. 2678–2683.
DOI: https://doi.org/10.1109/TIP.2011.2131660

[27] K. Bahrami, A. C. Kot, A Fast Approach for No-Reference Image Sharpness Assessment Based on Maximum Local Variation, IEEE Signal Process. Lett., vol. 21, no. 6, June 2014, pp. 751–755.
DOI: https://doi.org/10.1109/LSP.2014.2314487

[28] S. Bosse, D. Maniry, K.-R. Muller, T. Wiegand, W. Samek, Deep Neural Networks for No-Reference and Full-Reference Image Quality Assessment, IEEE Trans. Image Process., vol. 27, no. 1, Jan. 2018, pp. 206–219.
DOI: https://doi.org/10.1109/TIP.2017.2760518

[29] S. Bianco, L. Celona, P. Napoletano, R. Schettini, On the Use of Deep Learning for Blind Image Quality Assessment, Signal Image Video Process, 2016, vol. 12, 8 pp.
DOI: https://doi.org/10.48550/ARXIV.1602.05531

[30] K. Zeng, Y. Wang, J. Mao, J. Liu, W. Peng, N. Chen, A Local Metric for Defocus Blur Detection Based on CNN Feature Learning, IEEE Trans. Image Process., vol. 28, no. 5, May 2019, pp. 2107-2115.
DOI: https://doi.org/10.1109/TIP.2018.2881830

[31] International Vocabulary of Metrology – Basic and general concepts and associated terms (VIM), 3rd edition. Online [Accessed 14 November 2024].
https://www.bipm.org/doi/10.59161/JCGM200-2012

[32] Optris, PI 1M: IR cameras for the metal industry. Online [Accessed 24 May 2024]
https://www.optris.com/en/product/infrared-cameras/pi-series/pi-1m/

[33] V. Medici, M. Martarelli, N. Paone, (+ another 8 authors), Integration of Non-Destructive Inspection (NDI) systems for Zero-Defect Manufacturing in the Industry 4.0 era, IEEE Int. Workshop on Metrology for Industry 4.0 & IoT (MetroInd4.0&IoT), Brescia, Italy, 6-8 June 2023, pp. 439–444.
DOI: 10.1109/MetroInd4.0IoT57462.2023.10180016

[34] P. Catti, M. Ntoulmperis, V. Medici, M. Martarelli, N. Paone, W. van de Kamp, N. Nikolakis, K. Alexopoulos, Quality control in manufacturing through temperature profile analysis of metal bars: A steel parts use case, Procedia CIRP, vol. 129, 2024, pp. 205–210.
DOI: https://doi.org/10.1016/j.procir.2024.10.036